



Land Surface Processes Simulation Over Thar Desert in Northwest India

P. RAJA,¹ C. V. SRINIVAS,³ K. B. R. R. HARI PRASAD,³ and NILENDU SINGH⁴

Abstract—Land surface processes in data scarce arid north-western India and their influence on the regional climate including monsoon are now gaining enhanced scientific attention. In this work the seasonal variation of land surface parameters and surface-energy flux components over *Lasiurus indicus* grassland system in Thar Desert, western India were simulated using the mesoscale WRF model. The data on surface fluxes from a micrometeorological station, and basic surface level weather data from the Central Arid Zone Research Institute's experimental field station (26°59'41"N; 71°29'10"E), Jaisalmer, were used for comparison. Simulations were made for typical fair weather days in three seasons [12–14 January (peak winter); 29–31 May (peak summer), 19–21 August (monsoon)] during 2012. Sensitivity experiments conducted using a 5-layer soil thermal diffusion (5TD) scheme and a comprehensive land surface physics scheme (Noah) revealed the 5TD scheme gives large biases in surface fluxes and other land surface parameters. Simulations show large variations in surface fluxes and meteorological parameters in different seasons with high friction velocities, sensible heat fluxes, deep boundary layers in summer and monsoon season as compared to winter. The shortwave radiation is underestimated during the monsoon season, and is overestimated in winter and summer. In general, the model simulated a cold bias in soil temperature in summer and monsoon season and a warm bias in winter; the simulated surface fluxes and air temperature followed these trends. These biases could be due to a negative bias in net radiation resulting from a high bias in downward shortwave radiation in various seasons. The Noah LSM simulated various parameters more realistically in all seasons than the 5TD soil scheme due to inclusion of explicit vegetation processes in the former. The differences in the simulated fluxes with the two LSMs are small in winter and large in summer. The deep mixed layers are distributed in the northeastern parts in summer, northern areas in southwest monsoon and in southwestern parts during winter seasons and associated with the land-cover and vegetation dynamics. Our results present a baseline simulation study in this data scarce arid region.

Key words: Arid climate, WRF, land surface parameters, Noah, 5TD, micrometeorology.

1. Introduction

Given the vast extent of arid and semi-arid regions ($\approx 40\%$ of the earth's land surface), land-atmosphere interactions play an increasingly important role in understanding weather, climate and regional/global environmental change (NITYOGI *et al.* 2010). Arid and semi-arid regions are characterized by low rainfall, sparse but highly dynamic moisture driven vegetation growth, and high temperatures. The regional climate in the arid and semi-arid areas is dynamically coupled to the land surface processes. The Thar Desert situated in the north-western India is a highly populated desert region in the world. It is presently facing changing environmental factors such as precipitation variations, land use alterations and vegetation changes (GOSWAMI and RAMESH 2008). The associated changes in greenness fraction, albedo, surface roughness, net radiation, transport of heat and moisture fluxes, and temperature (CHARNEY 1975; MORAN *et al.* 1994; UNLAND *et al.* 1996) could significantly alter the land-atmosphere coupling in this region.

Modeling of the surface processes over arid eco-regions is very important to study the seasonal variation of various components of surface energy balance (SEB) and the energy fluxes in the context of expansion of arid areas (DICKINSON and HENDERSON SELLERS 1988). The seasonal nature of precipitation with large spatial variability in arid or semi-arid regions leaves a large effect on seasonal patterns of surface water and energy exchange (STEWART *et al.* 1994; UNLAND *et al.* 1996). Energy partitioning in arid and semi-arid regions is different from the humid

¹ ICAR-Central Arid Zone Research Institute, Jodhpur 342 003, Rajasthan, India.

² Present Address: ICAR-Indian Institute of Soil and Water Conservation, Research Centre, Udhamandalam 643 004, Tamilnadu, India.

³ Radiological Safety and Environment Group, Indira Gandhi Centre for Atomic Research, Kalpakkam 603 102, Tamilnadu, India. E-mail: venkatasrinivasc@yahoo.com; cvsri@igcar.gov.in

⁴ Centre for Glaciology, Wadia Institute of Himalayan Geology, 33 GMS Road Dehradun, Dehra Dun 248001, Uttarakhand, India.

areas on seasonal and interannual scales as the energy transport in these areas depends on the seasonality of precipitation and vegetation dynamics (HUIZHI and JIANWU 2012; FRANK *et al.* 2010). Given the large annual variability of rainfall in the arid regions, the factors controlling the seasonal and interannual variations of the heat fluxes in these areas need to be examined. Recent studies highlight the requirement of accurate measurements of land surface properties: vegetation and soil moisture dynamics, surface energy fluxes and other micrometeorological and biophysical parameters and realistic models for improved understanding of the land–atmosphere interaction and the local and regional climate (BALDOCCHI *et al.* 2001; KABAT *et al.* 2004; ZENG *et al.* 2012; WANG *et al.* 2014; LIVNEH *et al.* 2011; YANG 2004). Land surface processes in tropical regions assume importance as weather and climate in these regions is highly influenced by tropical convection. Micrometeorological observation systems facilitate measurement of the exchange of radiation, energy and water in a local-scale footprint (0.5–1.0 km²) useful in characterization of the land surface processes (GOEL and SRIVASTAVA 1990; VERNEKAR *et al.* 2003; BHATTACHARYA *et al.* 2009). In the tropical to sub-tropical Indian context a few micrometeorological experiments such as MONTBLEX-90 (SIKKA and NARASIMHA 1995) along the region of monsoon trough, LASPEX-97 (VERNEKAR *et al.* 2003) in the semi-arid region of Gujarat have been conducted to study the land surface and boundary-layer processes.

Northwestern India is affected by rapid soil degradation, vegetation loss (RAVI and HUXMAN 2009) and exhibits large seasonal differences in vegetation, agriculture systems, rainfall and soil moisture. Agriculture and cropping in this area starts with the monsoon rains with major harvesting in winter or early spring (USDA 1994). The vegetation of this region comprises mainly dry open grassland that remains green only during monsoon months (mid-July to end of September) (RAHMANI and SONI 1997) and the rainfall is limited (150–200 mm) and mainly monsoon dependent. Though, this arid region in India is known to have a strong influence on the regional monsoon climate (BOLLASINA and NIGAM 2011) the surface fluxes from this area are not studied much. It is important to study the implications of seasonal

variation in vegetation and rainfall in different land surface processes (viz., albedo, net-available energy, heat and moisture fluxes, evaporation and evapotranspiration) in the local and regional climate. Mesoscale atmospheric models are preferred to simulate the land biosphere atmosphere interactive processes for studying the regional climate as they incorporate detailed land surface physics and the advective transport of energy fluxes (AVISSAR and PIELKE 1989; CHEN *et al.* 2001; SANJAY 2008; JIMENEZ *et al.* 2012).

The objective of this work is to study how the sparse vegetation of the dry and grassland system in the Thar Desert region of northwest India interacts with the southwest monsoon in modulating the energy fluxes using a mesoscale atmospheric model and observations gathered using Satellite linked (INSAT) Agro-meteorological stations (AMS) in the region. Towards this objective, two land surface physics parameterizations in the model are tested for reproducing the diel cycle of surface heating, evaporation, surface fluxes, etc.

2. Data, Methods and Simulations

2.1. Study Area

The study area is an arid and desert region of Jaisalmer in Rajasthan of northwest India (Fig. 1). This region is characterized by highly variable and low annual precipitation (100–300 mm), extremes of temperatures (−3 to 48 °C), high wind speed (8–9 ms^{−1}), and long sunshine hours (~9.4 h d^{−1}) which characterize a very large evaporative demand. Because of poor rainfall, soil moisture stress is an impediment to vegetation growth. The soils are loose, sandy to sandy loamy with excess permeability (>25.4 cm h^{−1}) and moderate to large water retention capacity (SHYAMPURA *et al.* 2002). Rainfall is received during a short duration in southwest monsoon with about 15 rainfall events and the supply of moisture lasts for a limited period of 90 days only. Low humidity, combined with strong wind regime, leads to advection, a phenomenon that causes evaporation loss more than the energy actually available through solar radiation (LEUNING *et al.* 2012).

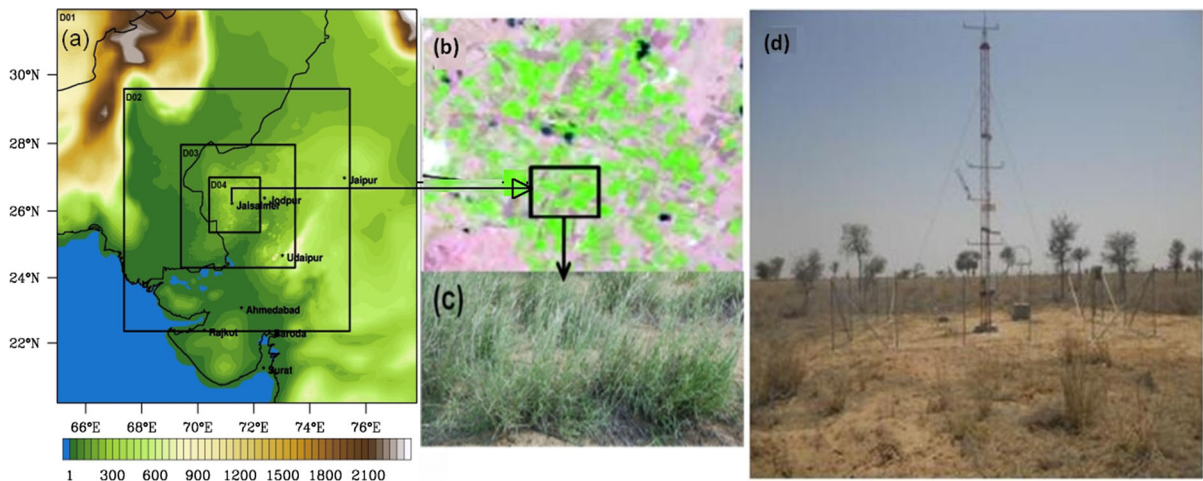


Figure 1

Location map of the study area: **a** Modelling domains used in ARW surrounding Jaisalmer, Rajasthan in the arid northwestern India, **b** experimental site at Chandan (CAZRI) (true color composite from Landsat-7 (ETM+) on over grassland at peak growth stage), **c** field photograph of grass growth pattern, **d** and box in panel 'c' denotes the location of the micrometeorological station

2.2. Observations

A 10 m micrometeorological tower with satellite based (INSAT: Indian National Satellite) data transmission facility was installed at Central Arid Zone Research Institute (CAZRI) experimental area (Fig. 1d) at Chandan (26°59'N, 71°20'E). The tower has a fetch ratio of approximately 1:50 (fetch from all directions is over 500 m) for continuous and automated measurements of components of radiation balance, Bowen ratio energy balance (BREB) and water balance (RAJA *et al.* 2013; BHATTACHARYA *et al.* 2013).

The details of various sensors are described in BHATTACHARYA *et al.* (2009). The sensors consist of four-component net radiometer (at 4 m) (Kipp and Zonen, Delft, The Netherlands), two-depth (at 0.1 and 0.2 m) soil heat flux plates (HFP01SC, Radiation and Energy Balance System Inc., USA), three-height air temperature and relative humidity probes with a shielded and aspirated sensor (HMP-45C, Campbell scientific, Logan, USA) and anemometer for wind speed and direction (KDS-131, KEPL, India) (at 1.25, 2.5 and 7.5 m), three-depth soil thermometers (KDS-031, KEPL, India) (0.05, 0.2 and 0.45 m) and rain-gage of tipping bucket type (KDS-071, KEPL, India). In addition, monthly volumetric sampling of soil moisture was carried out from three depths (0.05, 0.2, 0.45 m) near the tower. A 25-channel data logger (DSAWSKM1-W, KEPL, India) logged data every

second which were averaged over 30 min and stored in the data logger. The half-hourly micrometeorological data on radiation and energy balance components, winds and air temperature recorded during January to December 2012 in arid grassland ecosystem are used for comparison with model results. In addition, the sensible and latent heat flux reanalysis data at regional-scale ($2/3^\circ \times 1/2^\circ$ spatial resolution) was obtained from land surface products of MERRA (Modern Era Retrospective-analysis for Research and Applications) for comparison of model derived fluxes averaged over inner domain. MERRA is a NASA reanalysis for the satellite era using a major new version (V5) of the Goddard earth observing system (GEOS) data assimilation system (DAS).

2.3. Data Analysis

The processing of AMS mast data was carried out using 'Fluxsoft' software developed at Space Applications Centre (ISRO) (BHATTACHARYA *et al.* 2009). The instantaneous energy balance components are used for model comparison. Micrometeorological components were computed from the ratio of vertical gradients of air temperature and actual vapor pressure (converted from relative humidity and air temperature data) from the sensors placed at 2.5 and 7.5 m heights.

The energy balance approach (ARYA 2001) was based on the assumption that at the surface-atmosphere interface and the net radiation (R_n) is partitioned into sensible heat flux (H), latent heat flux (LE), ground heat flux (G) and metabolic or storage energy in the vegetation canopy (ΔQ).

$$R_n = H + LE + G + \Delta Q \quad (1)$$

$$R_n = RS_{in} - RS_{out} + RL_{in} - RL_{out} \quad (2)$$

RS and RL are shortwave (SW) and longwave (LW) radiation, respectively. The 'in' and 'out' are radiative flux directions. The storage heat of the canopy is being ignored in diel or seasonal cycle, with the assumption that the amount of energy stored during the heating is being released during the cooling cycle and also because of the short, open canopy vegetation. The amount of metabolic heat is usually negligible as compared to other components. Neglecting these energy terms, the Eq. (1) can be rearranged as:

$$R_n - G = AE = H + LE \quad (3)$$

AE is the net available energy. The H and LE are computed using simple aerodynamic approach following Monin–Obukhov Similarity Theory (MOST). In this approach the transfer of mass and energy from vegetation to atmosphere and vice versa takes place in accordance with concentration gradient of the respective quantity and the aerodynamic resistance between the source and sink (DYER 1974). First, the zero plane displacement (d) and roughness length (z_0) were computed from plant height (h) using simple empirical relationships: $d = 0.65 \times h$ and $z_0 = 0.1 \times h$ as given in CAMPBELL and NORMAN (1998). The vapor pressure (e), specific humidity (q), air density (ρ), etc. were computed from the tower measurements of temperature, RH and atmospheric pressure using standard psychrometric equations. The stability corrected aerodynamic resistance was calculated following DYER and HICKS (1970). An iterative technique was applied by initializing stability factor $\psi = 1$ and $L = 0$ (neutral stability condition). The H , u_* and L were computed following Eqs. (4–8), respectively. The iteration was repeated till the assumed L becomes nearly equal to the computed L (at 0.001 level of precision). The final

value of L was used for the computation of H and LE flux.

The aerodynamic resistance was estimated from wind speed and roughness parameters using the logarithmic wind profile equation. Solution of logarithmic equation is simple under neutral stability condition. However, absolute neutral stability cannot be assumed always because very often, there is a thermal gradient in either direction in the vertical profile within the lower boundary-layer. In the present study, stability corrected aerodynamic resistance was determined by solving the auto-correlation assuming Monin–Obukhov's Similarity Theory (MOST) following the approaches of (DYER 1974; BELJAARS and HOLTSLAG 1991; DE BRUIN *et al.* 2000).

The transfer of sensible and latent heat is expressed as:

$$\text{Sensible Heat Flux (H)} = -\rho C_p \theta_* u_* \quad (4)$$

$$\text{Latent Heat Flux (LE)} = -\rho q_* u_* \quad (5)$$

where, ρ = air density (kg m^{-3}), C_p (specific heat of air) = $1000 \text{ J kg}^{-1} \text{ K}^{-1}$, λ = latent heat of vaporization of water ($2.45 \times 10^6 \text{ J kg}^{-1}$), θ_* = temperature scale, q_* = humidity scale and u_* = frictional velocity (scale of mechanical turbulence).

The terms: u_* , θ_* and q_* are expressed as:

$$u_* = \frac{ku}{\ln[(Z_m - d)/Z_{om}] - \psi_m(\tau_{z_m}) + \psi_m(\tau_{z_{om}})} \quad (6)$$

$$\theta_* = \frac{k\theta}{\ln[(Z_T - d)/Z_{oh}] - \psi_h(\tau_{z_h}) + \psi_h(\tau_{z_{oh}})} \quad (7)$$

$$q_* = \frac{kq}{\ln[(Z_q - d)/Z_{oq}] - \psi_q(\tau_{z_q}) + \psi_q(\tau_{z_{oq}})} \quad (8)$$

where d = zero plane displacement (m), z_0 = roughness length (m), ψ_m , ψ_h and ψ_q are dimensionless stability functions, and z = height (m). The subscripts m , h and q stand for momentum, vapor and sensible heat fluxes, respectively. The stability functions Ψ is the integration of the dimensionless profiles ' ϕ ' and are a function of Monin–Obukhov similarity length (L) or Z/L (XU and QIU 1997),

$$L = -\rho \frac{C_p T_{abs} u_*^3}{kgH} \quad (9)$$

where, ρ = air density (kg m^{-3}) calculated from atmospheric pressure, RH (relative humidity) and temperature, T_{abs} = absolute temperature, C_p = specific heat of air = $1005 \text{ J kg}^{-1} \text{ K}^{-1}$, and g = acceleration due to gravity = 9.81 m s^{-2} .

2.4. Model Description

The Advanced Research WRF (ARW) mesoscale atmospheric model based on Eulerian mass dynamical core developed by NCAR, USA (SKAMAROCK *et al.* 2008) is used to simulate the surface fluxes and surface layer variables in this study. In recent times this model is widely used to investigate the impact of land surface processes on regional climate over various areas (KAR *et al.* 2014; SRINIVAS *et al.* 2014; BOLLASINA and SUGAM 2011). The model predicts three-dimensional wind, perturbation quantities of potential temperature, geopotential, surface pressure, turbulent kinetic energy and scalars (water vapor mixing ratio, cloud water etc.). The model includes a number of physics parameterizations for the simulation of land-biosphere processes, boundary-layer turbulence, convection, cloud micro-physics and radiation transfer in the atmosphere. The vertical coordinate of the model is terrain following hydrostatic pressure and the model horizontal grid is Arakawa staggered C-grid. The model can be configured to any region with dynamical nesting and using suitable physics parameterizations to resolve various scales of atmospheric processes.

2.5. Numerical Simulations

The ARW model is configured with four interactive nested domains (Fig. 1a). The outer domain covers northwest India and Pakistan with 54×55 grid cells and a cell size of 27 km, the second domain covers Rajasthan, northern Gujarat and southwestern Pakistan with a 100×100 grid cells and a cell size of 9 km, the third domain covers the northwest Rajasthan with 151×151 grid cells and a cell size of 3 km, and the fourth domain covers the Jaisalmer region around Chandan with 202×202 grid cells and cell size of 1 km. Simulations were conducted for typical fair

weather days in three seasons (12–14 January in Winter, 29–31 May in Summer, 19–21 August in Southwest monsoon of year 2012). The model is integrated for 48-h periods starting from 00 UTC/0600 IST on these dates (00 UTC 12 Jan, 00 UTC 29 May, 00 UTC 19 August 2012) with initial and boundary conditions taken from the 3-dimensional 3-hourly National Centers for Environmental Prediction (NCEP) Global Forecasting System (GFS) meteorological analysis and forecasts available at 0.5° ($\approx 50 \text{ km}$) resolution. The selected model physics parameterizations are the Kain-Fritsch scheme (KAIN and FRITSCH 1993) for convection, WRF single moment (WSM6) for cloud microphysics, Yonsei University (NOH *et al.* 2003; HONG *et al.* 2006) non-local scheme for Planetary Boundary Layer (PBL) diffusion, MM5 similarity theory (ZHANG and ANTHES 1982), RRTM scheme for longwave radiation (MLAWER *et al.* 1997; DUDHIA 1989) scheme for shortwave radiation processes. The RRTM is a spectral band scheme using correlated- k method to accurately simulate longwave processes due to atmospheric constituents. The Dudhia shortwave scheme computes downward solar flux considering absorption and reflection of clouds, clear-sky scattering, absorption of water vapor, surface slope and shading effects. No cumulus convection scheme is employed for the fine domains 3 and 4. For each season case, simulations are conducted with Noah land surface scheme (CHEN *et al.* 2001; TEWARI *et al.* 2004) and 5-layer soil thermal diffusivity model (5TD) (DUDHIA 1996) to study model sensitivity to land surface physics. These experiments are referred as Noah, 5TD, respectively.

The Noah land surface scheme (CHEN and DUDHIA 2001) computes soil temperature and moisture in 4 layers (0–10, 10–20, 20–40, and 40–100 cm), including canopy moisture, snow cover and soil physics which includes evapotranspiration, vegetation categories, root zone, soil drainage, runoff, and soil texture. It computes the sensible (H), latent heat (LE) fluxes and temperature at surface level. These fluxes are transported throughout the boundary layer and thus influence the growth and decay of the boundary layer (CHEN and DUDHIA 2001; MIAO *et al.* 2009).

Surface sensible (H) and latent (LE) heat flux provided by Noah LSM are stated as,

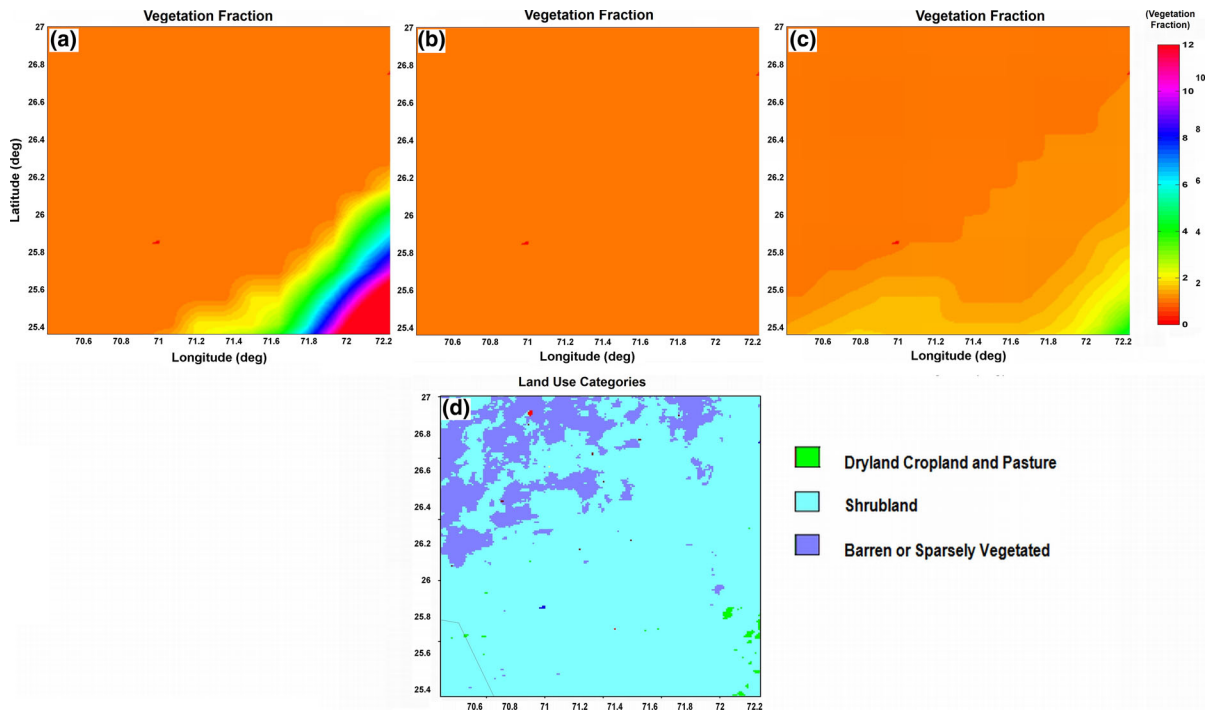


Figure 2
Vegetation fraction in **a** winter, **b** summer, **c** SW monsoon season, **d** land-cover in the study area

$$H = \rho c_p C_h u (T_{\text{sfc}} - T_{\text{air}}), \quad (10)$$

$$LE = \rho_d c_p C_h u (q_{\text{sfc}} - q_{\text{air}}), \quad (11)$$

where, ρ , ρ_d is the density of moist and dry air; c_p is the specific heat for air at constant pressure; C_h is the surface-layer turbulent exchange coefficient, u is the mean wind speed, q_{air} , T_{air} are specific humidity and temperature at the first model level, T_{sfc} , q_{sfc} are the surface temperature and specific humidity. The 5-layer soil model (DUDHIA 1996) solves the thermal diffusivity equation with 5 soil layers (1, 2, 4, 8 and 16 cm). The energy budget includes radiation, sensible and latent heat fluxes. It treats the snow cover, soil moisture fixed with a land use and season dependent constant value and explicit vegetation effects are not considered.

The US Geological Survey (USGS) terrain, 24-category land use and the food and agriculture organization (FAO) 16-category soil texture are interpolated from the original 5-arcminute, 2-arcminute and 30-arcsec datasets to the model grids 1, 2, 3 and 4, respectively. The vegetation fraction and background

surface albedo data are adopted from the NCEP monthly climatological datasets available at 0.1448° horizontal resolution (GUTMAN and IGNATOV 1997; CSISZAR and GUTMAN 1999). The land use classes and seasonal changes in green vegetation fraction in the innermost domain are presented in Fig. 2. The initial soil moisture and temperature in the LSMs are defined from NCEP global data assimilation system (GDAS) which follows a full self-cycling of soil moisture and temperature.

The YSU PBL scheme computes the vertical diffusion in the atmospheric boundary layer with first-order following a k -profile method and inclusion of counter gradient fluxes to account for non-local transport of heat and moisture fluxes. The friction velocities and exchange coefficients for the calculation of surface heat and moisture fluxes are computed using MM5 surface layer scheme which follows an iterative procedure using stability correction functions from (PAULSON 1970; DYER and HICKS 1970; WEBB 1970). These fluxes serve as boundary conditions for computing the vertical diffusion in the PBL.

The surface layer scheme couples the fluxes of heat, moisture and momentum from the model surface to the boundary layer above. Hence, the land surface scheme influences the predictions of the surface fluxes and the evolution of state variables in the atmosphere. Accurate prediction of surface fluxes and surface layer variables by mesoscale models is important as these quantities ultimately influence the prediction of PBL profiles and the model thermodynamics influencing the model predictions of several weather phenomena.

3. Results and Discussion

The dynamics of vegetation in the study region associated with monsoon rainfall controls the surface energy fluxes and other surface variables. The results of simulations are analyzed from the model innermost grid with 1-km resolution. The variables analyzed include shortwave (SW) radiation, friction velocity (momentum flux), surface energy fluxes (sensible and latent heat), 10 m winds, 2 m air temperature and mixing ratio and PBL heights in different seasons. The parameters taken from vegetation (albedo, moisture availability, surface roughness, moisture content) and those specified from soil categories (reference soil moisture, wilting point moisture, saturation soil conductivity, saturation soil diffusivity and soil thermal conductivity) influence the evolution of surface energy fluxes in the simulations. Seasonal differences in vegetation, agriculture systems, rainfall and soil moisture in the year have implications on the land surface processes. The seasonal changes in vegetation in the model are represented through green vegetation fraction determined from normalized difference vegetation index (NDVI) (GUTMAN and IGNATOV 1997) which is computed using satellite remote sensing data. The simulations of various seasons are sensitive to the changes in the vegetation fraction data. The seasonal vegetation fraction in the model 4th grid (Fig. 2) shows that while the northwestern parts are always devoid of vegetation (vegetation fraction nearly zero due to desert sands), the southeastern parts have large seasonal variation in vegetation. The vegetation fraction in these areas varied from 12 to 3 % and the

areas are more densely vegetative during winter and monsoon seasons and dry in the summer season.

3.1. Radiation and Surface Energy Fluxes

The diel shortwave (SW) and longwave (LW) radiation cycle from model and observations are presented in Fig. 3. The shortwave radiation (SW) has nearly similar magnitude in both summer and monsoon seasons, however, the longwave radiation is slightly more in monsoon season. It is seen that the simulated LW is very high in summer ($350\text{--}400\text{ Wm}^{-2}$) and monsoon ($410\text{--}450\text{ Wm}^{-2}$) compared to the winter ($250\text{--}275\text{ Wm}^{-2}$) season. The SW radiation is underestimated in monsoon season, and overestimated in winter and summer. The SW radiation simulated by 5TD, Noah schemes are nearly similar as the Dudhia shortwave radiation scheme considers the effects of clear-sky scattering, absorption of water vapor and surface slope and shading effects only. Unlike the SW radiation there are few differences in the LW radiation simulated by 5TD and Noah schemes (Fig. 3), especially in the summer which could be due to differences in the infrared emission based on surface temperature and land-use type by the RRTM scheme. The infrared emission depends on the vegetation type and its density which varied seasonally in the simulation domain (Fig. 1). Except monsoon, there is a large underprediction of LW in both the winter and summer, and the estimates by Noah are considerably better with $\approx 25\%$ improvements over the estimates from 5TD. LW is sensitive to the emissivity, which is a seasonally varying parameter according to the variation in the vegetation density. The large underprediction of LW in the case of 5TD during summer and winter is due to considering a seasonal fixed value for emissivity. The Noah scheme simulates vegetation processes explicitly and thereby LW more realistically.

The evolution of diel surface sensible heat flux in the three seasons (Fig. 4a–c) shows relatively large heat fluxes in summer ($\approx 500\text{ Wm}^{-2}$) followed by monsoon ($\approx 400\text{ Wm}^{-2}$) and winter ($\approx 200\text{ Wm}^{-2}$). The large sensible heat fluxes occur in the study area in summer because of dry and exposed soils that directly emit longwave radiation thus warming the

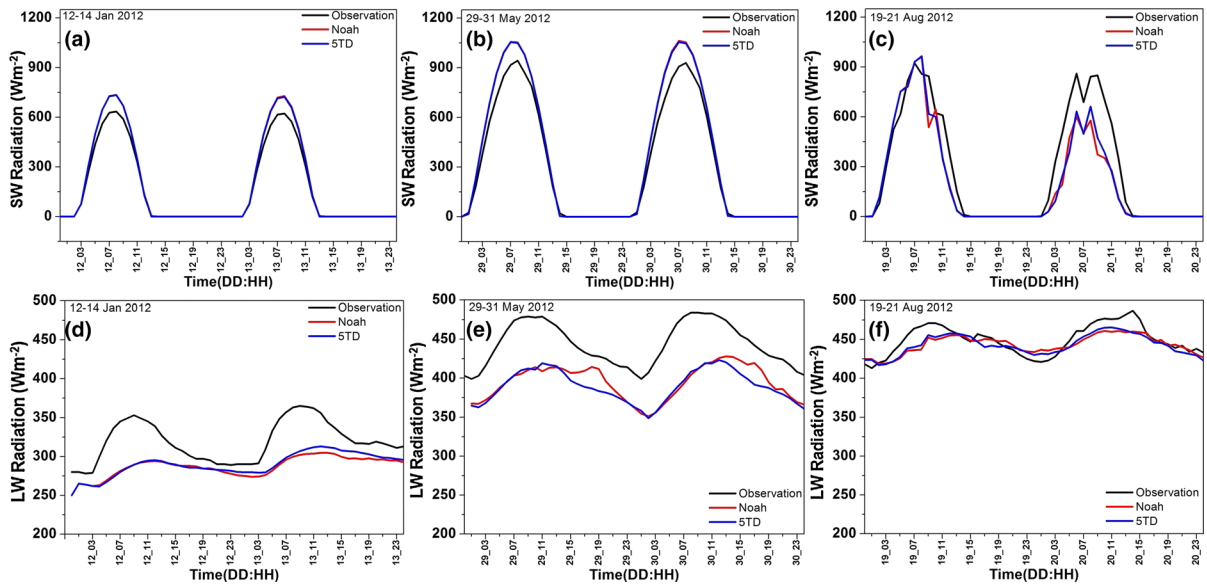


Figure 3

Diurnal variation of simulated short and longwave radiation (Wm^{-2}) along with observations for **a, d** winter **b, e** summer **c, f** SW monsoon season. *Top panels* are for shortwave and *bottom panels* are for longwave radiation. Noah, 5TD denote the simulation outputs using Noah and 5TD schemes respectively

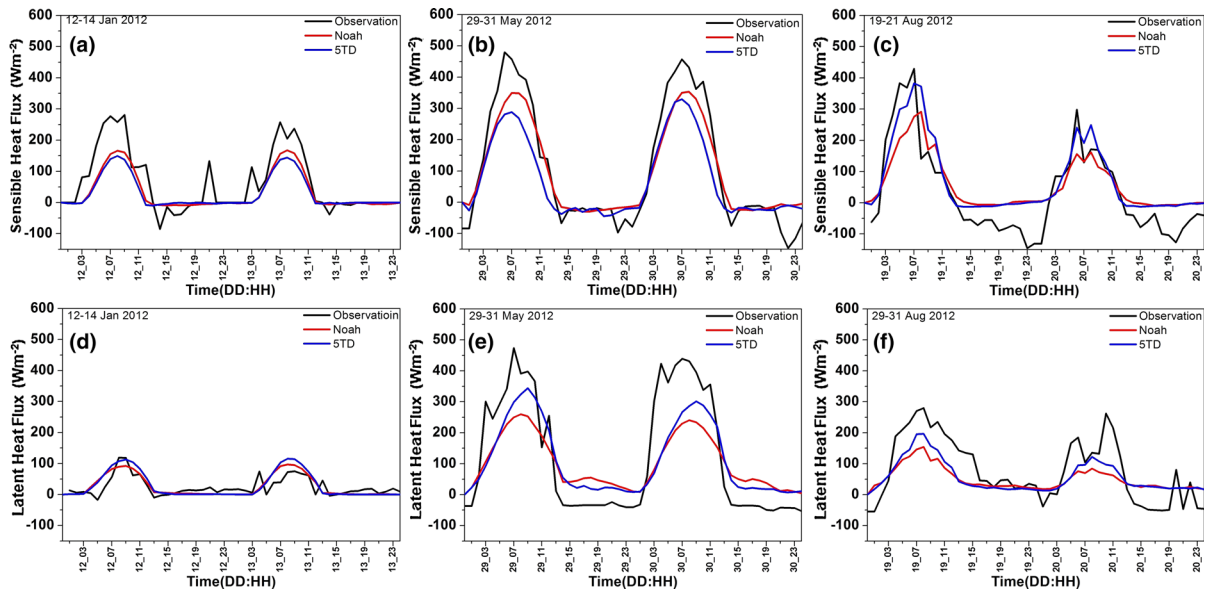


Figure 4

As in Fig. 3, but for surface energy fluxes (Wm^{-2}). *Top panels* represent the sensible heat and *bottom panels* represent latent heat flux

surface layer of atmosphere. The heat fluxes in summer are nearly thrice larger than those in winter. The latent heat fluxes (Fig. 4d-f) are larger in

summer (400 Wm^{-2}) and monsoon (250 Wm^{-2}) compared to winter (100 Wm^{-2}). The growth in vegetation in response to monsoon rainfall (Fig. 2)

and soil moisture reduced the albedo, increased energy absorption, and thus reduced the sensible heat flux in monsoon and post-monsoon period. The large LE in summer at the observation site could be due to direct evaporation of pre-monsoon rainfall and due to thunder-storms in the region. The H at the observation site is about two times higher than LE in winter and monsoon season. A comparison of domain averaged heat fluxes from model and MERRA data (Fig. 5) shows a similar behavior of sensible heat flux at the regional scale in different seasons to that at Chandan, however, the latent heat is about three and ten times smaller than the sensible heat in winter and summer, respectively, and is slightly higher than the sensible heat in the monsoon season. This suggests the energy transport to atmosphere from this arid zone with barren lands occurs mainly by dry processes rather than through moisture transport. The high sensible heat transport is attributed to poor monsoon rainfall, low soil moisture and low vegetation and the results corroborate with similar studies from arid Northwest China (ZHOU *et al.* 2010; ZHANG *et al.* 2005). The higher latent heat during monsoon season is due to soil moisture refilling by rainfall and

associated moisture driven green grass growth, thus indicating seasonal vegetation controls the energy partitioning.

The Noah land surface scheme predicted comparatively higher sensible heat fluxes close to the observational estimates in all seasons than the multi-layer soil model and shows $\sim 15\%$ improvement over those produced by the 5TD scheme. Though the 5TD scheme produced slightly better agreement of latent heat with observations at Chandan, it predicted higher latent heat relative to Noah at the regional scale (Fig. 5). The difference in simulated fluxes between the two LSM schemes is very small in winter but large in summer and monsoon season which is because the complete surface processes (canopy reflectance, evapotranspiration, dew or fog effect etc.) are not included in the simple 5TD soil model. This is evident particularly in the monsoon season where the soil model simulated relatively large latent heat flux compared to the Noah scheme, mainly because of not explicitly accounting for soil moisture and vegetation processes. Verification of surface fluxes at Chandan station shows a negative bias indicating underestimation of the fluxes

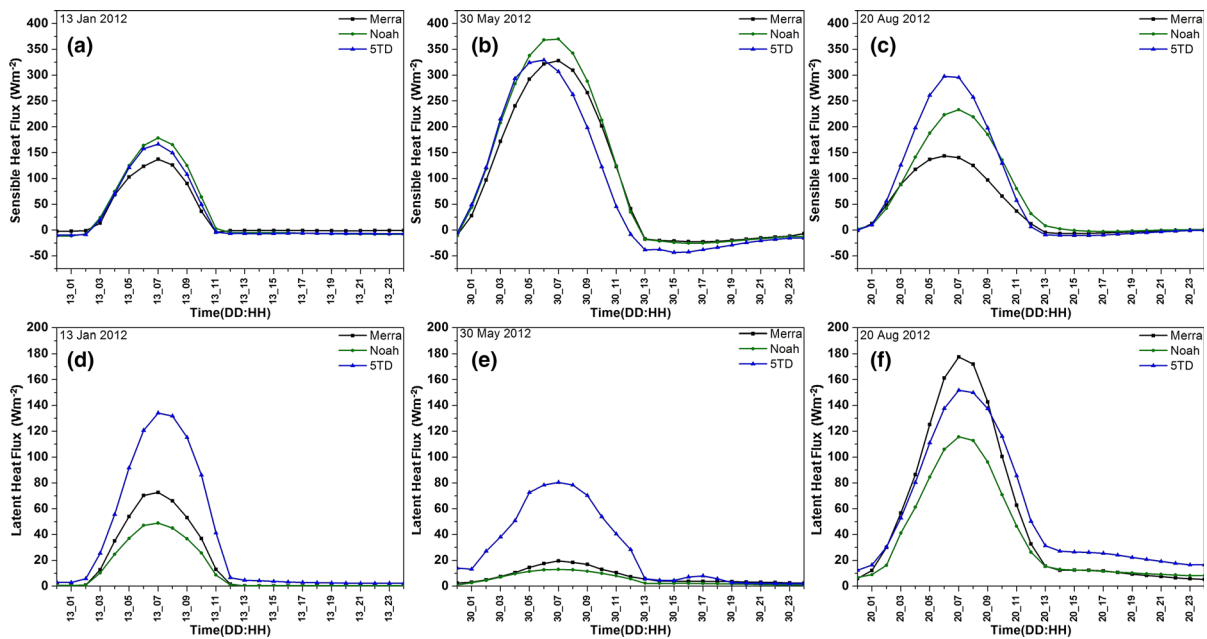


Figure 5

As in Fig. 3, but for regional surface energy flux (Wm^{-2}) along with MERRA observations. *Top panels* represent the sensible heat and *bottom panels* represent latent heat flux

by both the schemes. This negative bias in fluxes could be due to negative bias in net radiation resulting from a bias of $20\text{--}50\text{ Wm}^{-2}$ in downward shortwave radiation (RS_{in}). Both the land surface schemes could not represent the nocturnal downward fluxes found in the observations indicating clear weakness of both models.

3.2. Air Temperature and Humidity

The surface fluxes are transported and diffused in the boundary layer of the atmosphere and therefore influence air temperature and humidity. Both soil and air temperatures are high in summer, monsoon season compared to winter (Fig. 6) and followed the heat fluxes in the respective seasons. The large air ($\approx 45\text{ }^{\circ}\text{C}$) and soil ($\approx 58\text{ }^{\circ}\text{C}$) temperatures in the summer characterize the heat low of the southwest monsoon which develops over the north-western India before the onset of monsoon. In all seasons the diel cycle of air temperature (2 m) and soil temperature (0–30 cm layer) is very closely simulated by Noah scheme compared to the 5TD (Fig. 6) though the air temperature is slightly underestimated. Slight warm bias in winter and monsoon seasons and slight cold bias

Figure 7
Spatial variation of soil temperature ($^{\circ}\text{C}$) for **a, b** winter on 06 UTC/1200 IST 13 Jan 2012, **c, d** summer on 06 UTC/1200 IST 30 May 2012, **e, f** SW monsoon on 06 UTC/1200 IST 20 Aug 2012. *Right panels* are for Noah LSM and *left panels* are for 5TD scheme

in summer are found in soil and air temperatures. Both simulations and observations show large daily temperature ranges in summer ($\approx 20\text{ }^{\circ}\text{C}$) and winter ($\approx 15\text{ }^{\circ}\text{C}$) compared to the monsoon season ($\approx 10\text{ }^{\circ}\text{C}$) which is because of cloud activity in monsoon season. The better performance of Noah model for air temperature seems to be due to reproducing the soil temperature and sensible heat flux more accurately than the simple soil model. While the soil model produced large cold bias, the Noah scheme reduced the bias in summer soil temperatures (Fig. 6). The Noah scheme also simulated the seasonal variation in soil temperatures in good agreement with observations. The regional spatial soil temperature field simulated using the 5TD and Noah schemes (Fig. 7) shows the distribution of highest temperatures in summer and monsoon season and the lowest temperatures in winter over the western and north-western barren land areas having sparse vegetation.

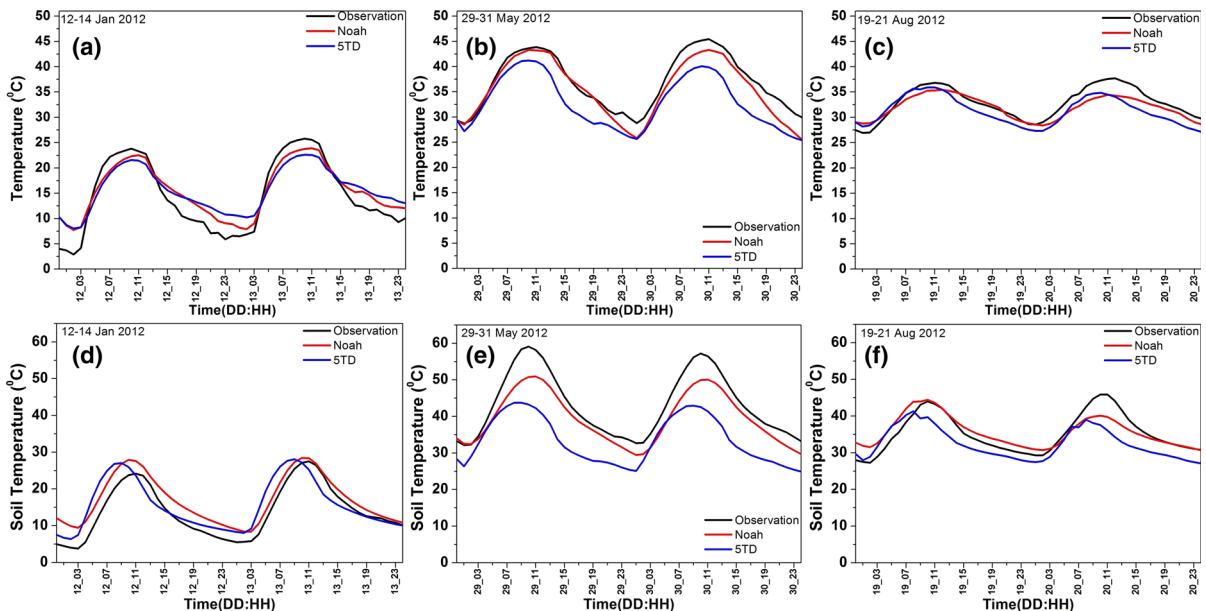
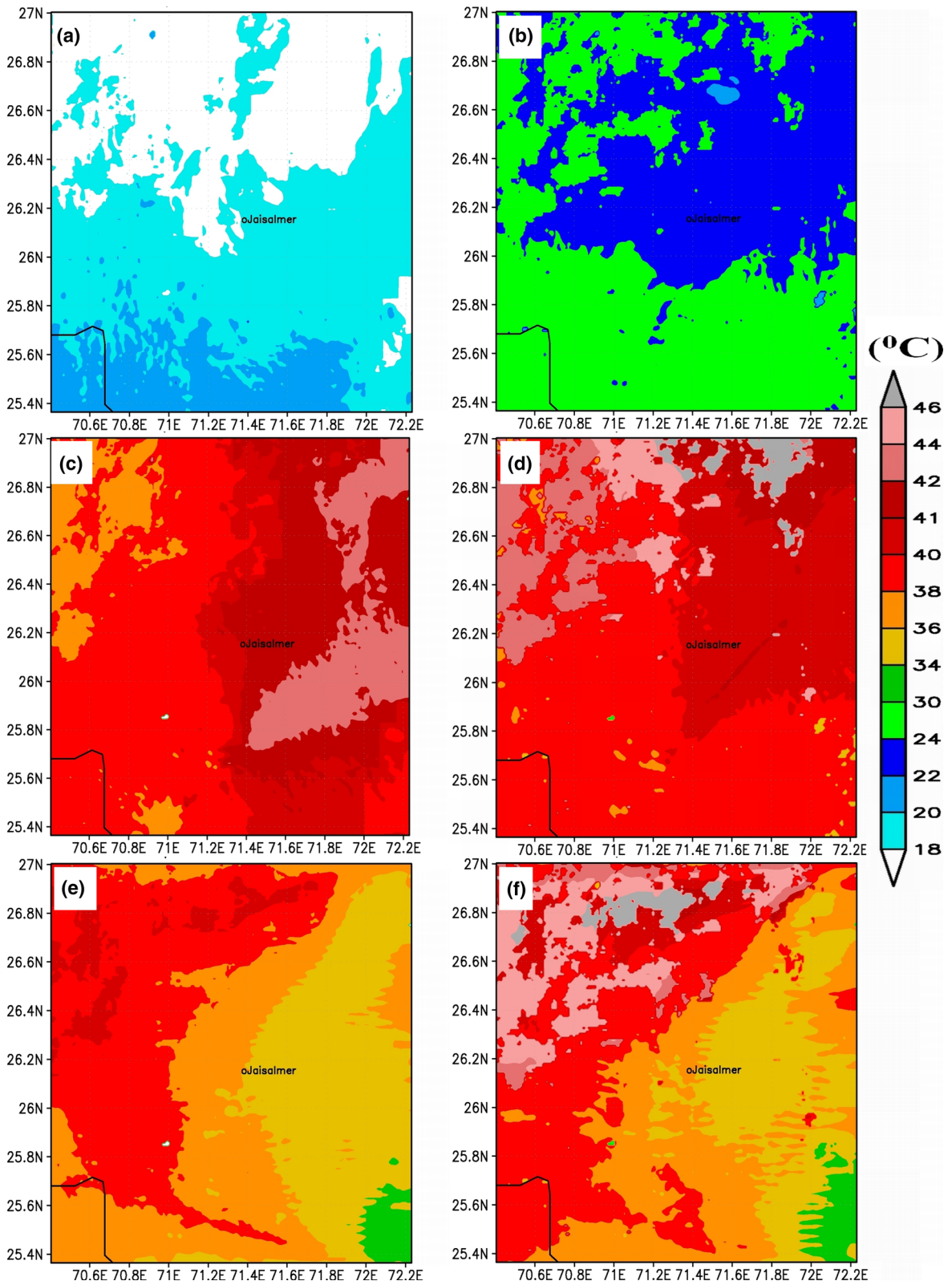


Figure 6

As in Fig. 3, but for air and soil temperature ($^{\circ}\text{C}$). *Top panels* represent the 2-m air temperatures and *bottom panels* soil temperatures



The 5TD scheme simulated systematically larger temperatures (Fig. 7a, c, e) relative to the Noah scheme (Fig. 7b, d, f) throughout the domain.

Both observations and simulation show higher humidity mixing ratio (2 m) during the monsoon season compared to other seasons (Fig. 8) due to large latent heat transport during the monsoon. The Noah scheme simulated the humidity in better agreement with observations than the 5TD which produced large humid bias in all the seasons. The better comparisons of humidity with Noah scheme are due to the explicit treatment of vegetation processes such as canopy effects, evaporation and evapotranspiration (CHEN and DUDHIA 2001).

3.3. Wind Field and Boundary Layer Height

Both observed and simulated winds at Chandan site are stronger during summer and southwest monsoon

season compared to winter (Fig. 9) and there is good agreement of simulated winds with observations using 5TD scheme. The Noah scheme produced relatively stronger winds in summer than the 5TD which would lead to transfer of higher momentum fluxes (u_*). The higher observed and simulated friction velocity (momentum flux) in summer and southwest monsoon as compared with winter (noah shown) could be due to the stronger surface level winds in these seasons. The daily variation in u_* with peak values during daytime and lowest values at night is well reproduced in the simulation and is in good agreement with observations. However, the model slightly overestimated momentum flux in summer. Overall, the low-level winds are better simulated by 5TD than Noah.

The spatial daytime simulated surface layer mesoscale flowfield at 10 m level corresponding to 0800 UTC/1400 IST (Fig. 10) shows the variation in wind patterns in different seasons. The daytime

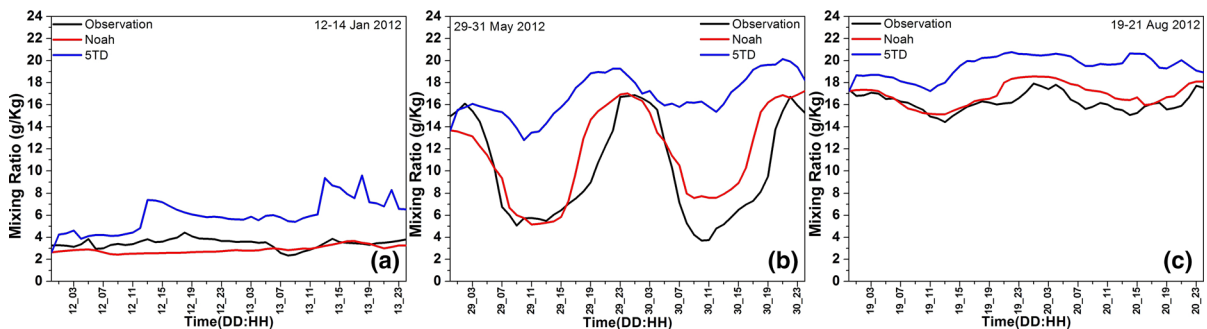


Figure 8

Diurnal variation of simulated 2-m mixing ratio (g/kg) along with observations for a winter b summer c SW monsoon season. Noah, 5TD denote the simulation outputs using Noah and 5TD schemes respectively

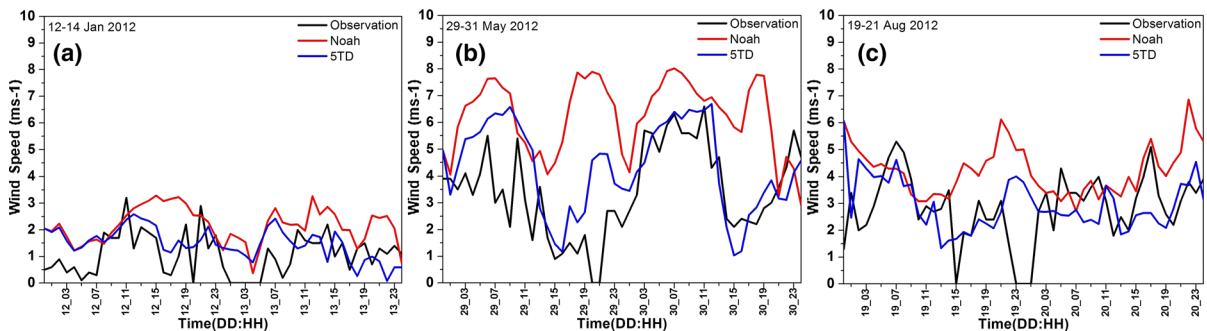


Figure 9

As in Fig. 8, but for 10-m wind speed (ms⁻¹)

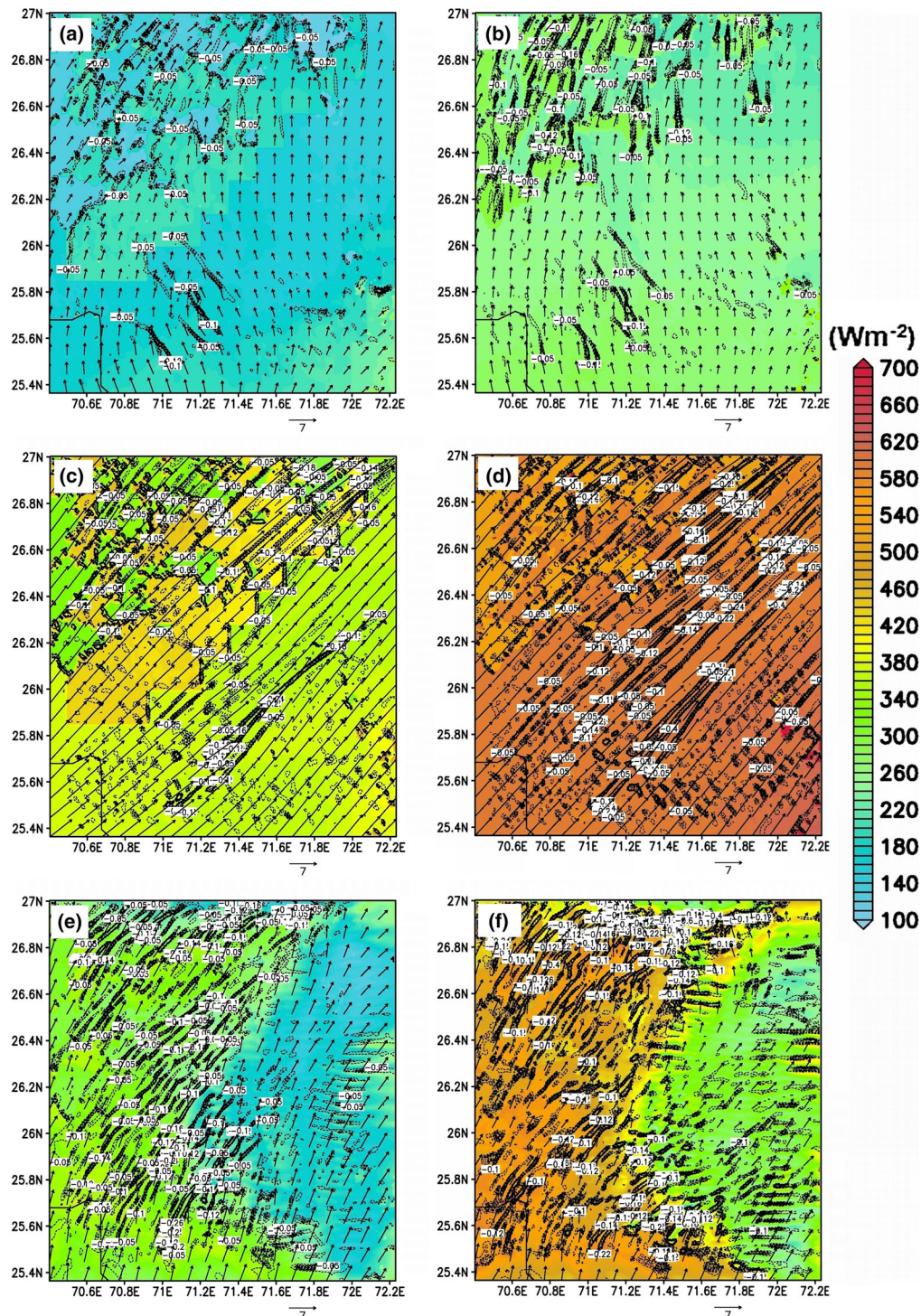


Figure 10

Spatial 10-m wind field (in vectors), total surface energy flux (Wm^{-2}) (in shaded) and flux convergence (s^{-1}) for a, b winter on 06 UTC 13 Jan 2012, c, d summer on 06 UTC 30 May 2012, e, f SW monsoon on 06 UTC 20 Aug 2012. Right panels are for Noah LSM and left panels are for 5TD scheme

surface layer winds are influenced by mesoscale southerly to southwesterly winds in the summer and winter, and by the large-scale southwesterly winds during southwest monsoon. Large spatial variability in winds is noticed between winter and summer in the study region. Also large diel variability of winds (wind direction) is seen in the summer and winter months (not shown) which could be due to generation of local winds due to spatial variation in land use and land cover (desert to agriculture lands). Appreciable differences in the spatial wind field are noticed in the southwestern parts in the winter season (Fig. 10a, b) and in the southwestern and eastern parts in the southwest monsoon (Fig. 10e, f) between the two simulations. The differences in the flow field and surface fluxes (sensible heat and latent heat) among the two land surface schemes lead to differences in advection of heat and moisture fluxes at the observation site in the two simulations. The simulations indicate stronger flux convergence (-0.1 to -0.4 s^{-1}) at the observation site in 5TD compared to Noah (-0.05 to -0.1 s^{-1}).

Simulated spatial PBL height (Fig. 11) shows formation of deep to very deep boundary layers (1800–2800 m) in summer which is due to extremely large sensible heat fluxes associated with sparse vegetation (Fig. 5) that control the degree of convective turbulence in this season. The PBL height is reduced during the monsoon (1500–2100 m) and post-monsoon (1300–1800 m) seasons due to development of vegetation driven by monsoon rainfall and decrease of heat fluxes. Large differences (i.e., location of deep layers vs shallow layers) are noted in the PBL height among the two LSMs in each of the seasons. The deep PBL layers are found in the northeastern parts in summer, in northern areas during southwest monsoon, and in southwestern parts during winter. The Noah scheme produced relatively deeper PBL layers than the 5TD scheme throughout the domain in all seasons (Fig. 11a–d). In the southwest monsoon season the 5TD scheme produced relatively deeper boundary layers compared to the Noah (Fig. 11e–f) which is confirmed by radiosonde observations at Jodhpur (26.30N, 73.01E). Simulated vertical profiles of mixing ratio and potential temperature corresponding to the radiosonde observation site at Jodhpur (Fig. 12) shows highly stable boundary

layer (in winter, neutral to stable boundary layers in summer and neutral layers (in monsoon seasons in the morning time. The vertical structure of the morning PBL (Fig. 12a–f) in all seasons is well simulated in Noah where as 5TD produced deeper layers in monsoon (Fig. 12b, e). The daytime profiles (Fig. 12g–l) show very deep boundary layers (≈ 1700 m) during summer and monsoon season and moderate layers (≈ 1200 m) during winter and that Noah produced relatively deeper layers compared to 5TD. The deep boundary layers in summer and moderate layers in monsoon are well simulated by Noah because of realistically simulating the surface energy fluxes accounting for the effects of rainfall, soil moisture accumulation, plant canopy and evapotranspiration processes. The deep boundary layers noticed in the western, northern and northwestern areas of the domain are because of large heat fluxes associated with barren lands and desert sands. The simulation using Noah scheme realistically produced the spatial variation in PBL height associated with land-cover/vegetation dynamics in the study region. The Noah scheme has produced relatively larger PBL height compared to the 5TD soil scheme and it realistically accounts the total upward heat fluxes.

The performance of the two land surface schemes is examined quantitatively by computing error statistics (bias, mean absolute error, root mean square error and correlation) with observations for all three seasons at Chandan station (Table 1). It has been found that in all three seasons, the Noah scheme produces a smaller error for various land surface parameters than the simple 5TD soil scheme which is most pronounced in reduction of the cold bias in temperature, humid bias in relative humidity, negative bias in sensible and latent heat fluxes, and cold bias in soil temperatures.

Further attribution needs both observational and modelling studies on all relevant physical mechanisms, which is challenging due to the scarcity of adequate observations in this arid region. The differences between observations and the WRF simulation highlight the need for improved observation network and designing suitable land-data assimilation. More in situ data will allow us to quantify the feedbacks between vegetation conditions and the surface heat fluxes and to

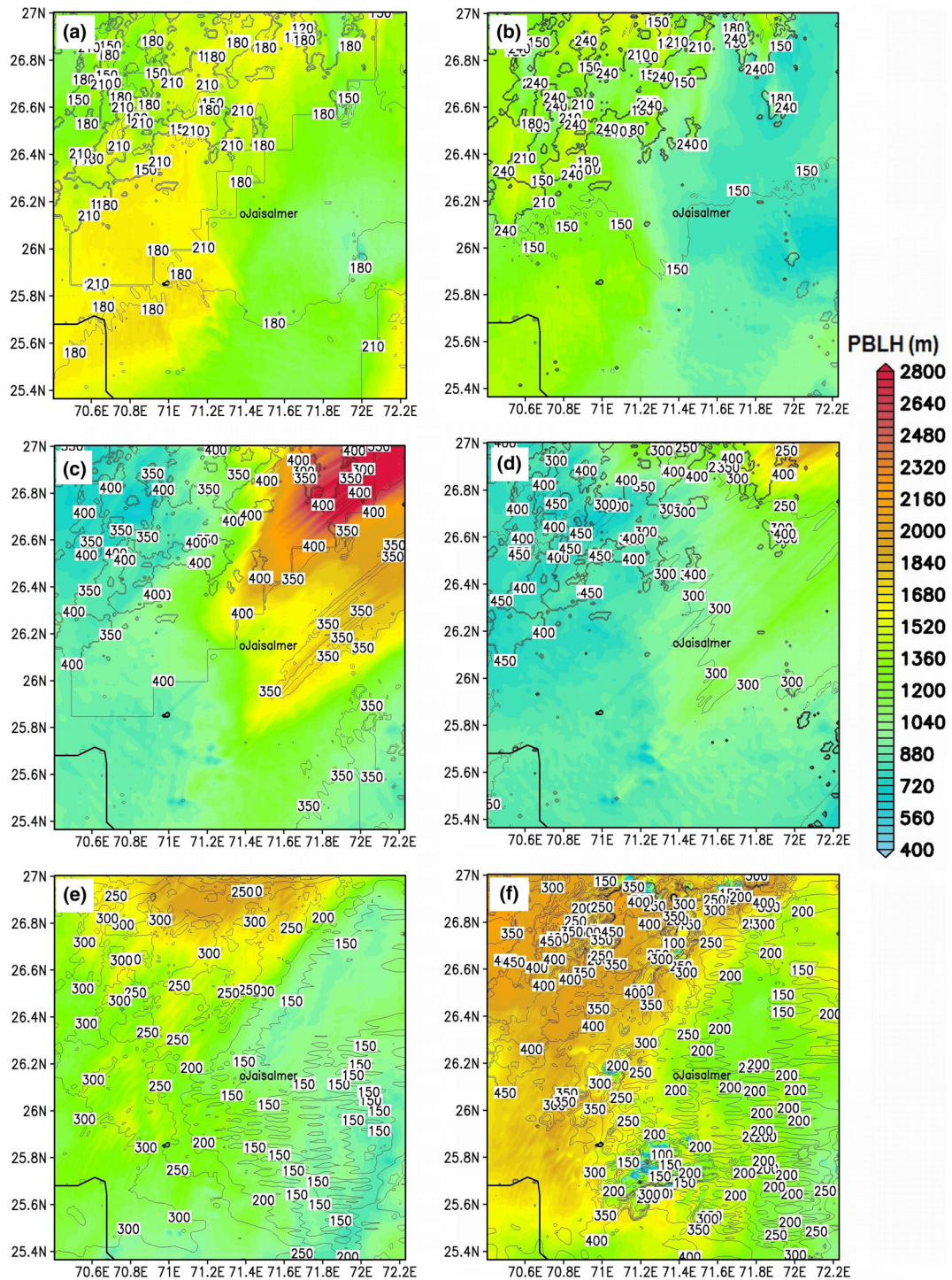


Figure 11

Spatial boundary layer height (in shaded), relative humidity (in contour) for **a, b** winter on 06 UTC 13 Jan 2012, **c, d** summer on 06 UTC 30 May 2012, **e, f** SW monsoon on 06 UTC 20 Aug 2012. Right panels are for Noah LSM and left panels are for 5TD scheme

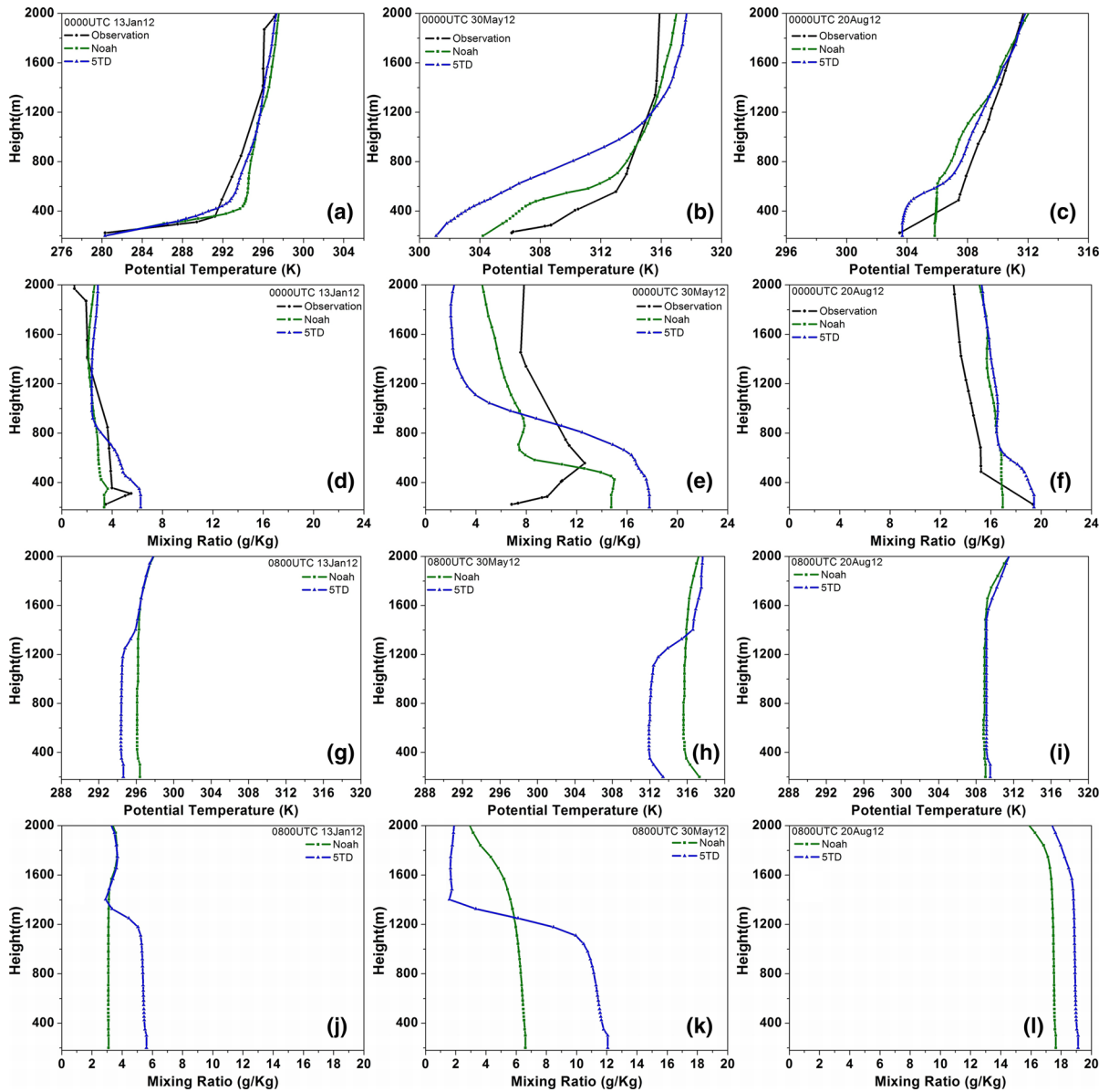


Figure 12

Comparison of simulated vertical profiles of mixing ratio q (g/kg) and potential temperature θ (K) with Radiosonde observations on 13 Jan 12 (winter), 30 May 12 (summer) and 20 Aug 12 (southwest monsoon). The first and third rows are for θ ; and second and fourth rows are for q . Panels a–f are for 0000 UTC and panels g–l are for 0800 UTC

have a more realistic parameterization of surface processes in atmospheric models. The gap in the simulated and observed parameters in the present study shows that accurate simulation of land surface processes: such as LE and H into the atmosphere, is essential for characterizing the land/atmosphere coupling that strongly affects the monsoon system.

4. Conclusions

Present study examined the evolution of the land surface parameters and their seasonal variation in the Thar Desert region of Rajasthan in western India using the ARW regional atmospheric model. Observations on micrometeorological variables and surface

Table 1

Error statistics of WRF simulations from the two LSM schemes for short and longwave radiation components, surface fluxes and surface meteorological variables at Chandan, Jaisalmer

Parameter	Season	Experiment	BIAS	MAE	RMSE	R
Temperature (°C)	Winter	Noah	0.96	2.19	2.53	0.98
		5TD	1.02	3.00	3.28	0.96
	Summer	Noah	-1.39	1.50	1.89	0.97
		5TD	-4.16	4.07	4.55	0.93
	Monsoon	Noah	-0.94	1.34	1.64	0.92
		5TD	-1.62	1.91	2.17	0.88
Relative humidity (%)	Winter	Noah	-10.32	11.04	14.58	0.89
		5TD	17.02	18.36	21.35	0.70
	Summer	Noah	6.27	8.08	10.20	0.92
		5TD	26.20	25.87	29.21	0.76
	Monsoon	Noah	4.51	5.53	6.69	0.89
		5TD	15.35	15.32	17.07	0.77
Wind speed (ms ⁻¹)	Winter	Noah	1.11	1.15	1.35	0.41
		5TD	0.43	0.83	0.95	0.24
	Summer	Noah	0.90	1.90	2.39	0.13
		5TD	-1.11	1.83	2.17	0.48
	Monsoon	Noah	-0.14	1.18	1.42	0.10
		5TD	-1.39	1.73	1.97	0.12
Short wave radiation (Wm ⁻²)	Winter	Noah	23.33	23.39	43.08	1.00
		5TD	22.40	22.54	41.58	1.00
	Summer	Noah	44.52	45.75	71.64	1.00
		5TD	43.36	44.63	69.71	1.00
	Monsoon	Noah	-71.76	86.46	149.94	0.92
		5TD	-68.24	82.06	138.80	0.93
Long wave radiation (Wm ⁻²)	Winter	Noah	-32.83	32.16	37.63	0.73
		5TD	-30.19	29.57	35.55	0.70
	Summer	Noah	-48.40	47.42	51.74	0.74
		5TD	-53.36	52.27	54.72	0.88
	Monsoon	Noah	-5.65	10.37	12.94	0.85
		5TD	-6.30	9.42	11.44	0.90
Sensible heat flux (Wm ⁻²)	Winter	Noah	-29.50	37.18	57.78	0.91
		5TD	-33.57	42.12	65.06	0.91
	Summer	Noah	-11.60	49.74	65.63	0.98
		5TD	-37.66	67.25	88.77	0.97
	Monsoon	Noah	23.87	66.36	82.24	0.89
		5TD	38.06	58.15	72.96	0.90
Latent heat flux (Wm ⁻²)	Winter	Noah	1.21	17.34	22.93	0.75
		5TD	4.06	19.70	25.71	0.78
	Summer	Noah	-24.91	102.45	119.86	0.92
		5TD	-14.23	82.70	101.65	0.90
	Monsoon	Noah	-29.43	64.63	78.51	0.86
		5TD	-22.35	55.87	67.32	0.86
Soil temperature (°C)	Winter	Noah	3.16	3.09	3.52	0.98
		5TD	1.74	3.07	3.96	0.87
	Summer	Noah	-3.67	3.65	4.27	0.98
		5TD	-9.77	9.57	10.47	0.90
	Monsoon	Noah	0.37	2.06	2.67	0.88
		5TD	-2.85	3.57	4.25	0.81

energy fluxes from a ISRO developed Agrometeorological station (AMS-ISRO) and a weather station at CAZRI experimental field, Chandan in Jaisalmer are

used for comparison. Two land surface physics schemes in ARW are evaluated with flux datasets. Large seasonal variations are found in the simulated

fluxes and surface meteorological parameters. The differences are attributable to the large seasonal differences in vegetation and rainfall at the study region. Results suggest that the Noah LSM reproduces various land surface parameters in better comparison with observations over simple soil diffusion model which is revealed from qualitative and quantitative comparisons for various land surface parameters. The daytime fluxes are higher by 40 % in summer, 25 % in monsoon compared to winter fluxes which model could correctly predict using Noah LSM. The high heat fluxes ($\approx 400\text{--}500 \text{ Wm}^{-2}$) in summer and monsoon season is due to poor monsoon rainfall, low soil moisture and consequent low vegetation that supports energy transfer mostly by sensible heat. The higher heat fluxes in these seasons are also because of strong advective heat transport to the observation site which is identified from wind field simulated by ARW model. Error statistics reveals that the model biases are reduced with Noah LSM for surface energy fluxes, temperature, winds and other variables. The biases in some of the parameters could be due to initial soil moisture and temperature fields initialized using NCEP analysis data. The model simulations of different land surface parameters using ARW with Noah LSM can be used for hydrologic and agricultural applications in the study region for crop planning purposes. Some of the areas which need improvements in simulations include: (1) reduction of surface insolation bias using a better radiation transfer model in WRF, (2) validation of sensible, latent and ground heat flux physics to account for issues of soil moisture-temperature initialization, (3) application of higher resolution vegetation and soil classes in the land surface physics, and (4) expansion of validation effort with other available station data sets in the study region. The simulations can be further refined using a local land data assimilation system by generating soil moisture and temperature measurements and using high resolution local land-use and soil cover data sets in the region which would be attempted in the future work.

Our study concludes that actions to rejuvenate the arid grasslands ($\sim 1/3$ of the entire region), will both facilitate a sustainable agro-ecological development and local climate benefits in this water scarce region. More accurate and long-term simulations of the

biophysical coupling between the land surface and the atmosphere are needed to help understand regional climate change and possible larger scale feedbacks between desert climate and the monsoon system in the southeast Asia.

Acknowledgments

The authors gratefully acknowledge Dr. B. Venkatraman (Division Head & Associate Director, RSEG/IGCAR) and Dr. R. Baskaran (Head, RIAS), IGCAR, Kalpakkam for providing all facilities to carry out numerical simulations at IGCAR. The micrometeorological observations used in the study are generated at Central Arid Zone Research Institute (CAZRI) under the project titled "Energy and Mass Exchange in Arid Grassland System" which forms a part of SAC national programme "Energy and Mass Exchange in Vegetative Systems (EME-VS)". Authors are thankful to the Director, Space Applications Centre (ISRO) for funding this project and Director, ICAR-CAZRI for providing facilities to carry out this work. Authors thank the anonymous reviewers for their technical comments which improved the content of this manuscript. Authors also thank Director, Wadia Institute of Himalayan Geology for providing facilities for surface flux computation through different micrometeorological methods.

REFERENCES

- ARYA, S. P. (2001), *Introduction to micrometeorology*. Academic Press, San Diego; 420 pp.
- AVISSAR, R., PIELKE R. A. (1989), *A parameterization of heterogeneous land surfaces for atmospheric numerical models and its impact on regional meteorology*. Mon. Weather Rev. 117, 2113–2136.
- BALDOCCHI, D., FALGE, E., GU, L., OLSON, R., HOLLINGER, D., RUNNING, S., ANTHONI, P., BERNHOFER, C., DAVIS, K., EVANS, R., FUENTES, J., GOLDSTEIN, A., KATUL, G., LAW, B., LEE, X., MALHI, Y., MEYERS, T., MUNGER, W., OECHEL, W., PAW, K. T., PILEGAARD, K., SCHMID, H. P., VALENTINI, R., VERMA, S., VESALA, T., WILSON, K., WOFSY, S. (2001), *FLUXNET: a new tool to study the temporal and spatial variability of ecosystem-scale carbon dioxide, water vapor, and energy flux densities*. Bull. Amer. Meteor. Soc. 82, 2415–2434.
- BELJAARS, A.C.M., HOLTSLAG, A.A.M. (1991), *Flux parameterization over land surfaces for atmospheric models*. J. Appl. Meteorol. 30, 327–341.

- BHATTACHARYA, B. K., GUNJAL, K., NANDA, M., PANIGRAHY, S. (2009), Protocol development of energy-water flux computation from AMS and Model development. SAC/RESA/ARG/EMEVs/SR/02/2009, Chapter 3, pp. 34–53, Space Applications Centre, Ahmedabad.
- BHATTACHARYA, B. K., SINGH, N., BERA, N., NANDA, M. K., BAIRAGI, G. D., RAJA, P., BAL, S. K., MURUGAN, V., KANDPAL, B. K., PATEL, B. H. JAIN, A., PARIHAR J. S. (2013), Canopy-scale dynamics of radiation and energy balance over short vegetative systems. Scientific Report SAC/EPSA/ABHG/IGBP/EME-VS/SR/02/2013, pp.97, Space Applications Centre, Ahmedabad.
- BOLLASINA, M., NIGAM, S. (2011), *Modeling of regional hydroclimate change over the Indian subcontinent: impact of the expanding Thar Desert*. J. Climate, 24, 3089–3106.
- CAMPBELL, G. S., NORMAN, J. M. (1998), Introduction to environmental biophysics. Springer Science-Business Media Inc. New York, pp. 71.
- CHARNEY, J.G. (1975), *Dynamics of deserts and drought in Sahel*. Quart. J. R. Meteorol. Soc. 101, 193–202.
- CHEN, F., DUDHIA, J. (2001), *Coupling an advanced land surface-hydrology model with the Penn State-NCAR MM5 modeling system. Part I: model implementation and sensitivity*. Mon. Weather Rev. 129, 569–585.
- CHEN, F., PIELKE, R. Sr., MITCHELL, K. (2001), Development and application of land-surface models for mesoscale atmospheric models: problems and promises. Observation and modeling of the land surface hydrological processes, in : LAKSHMI, V., ALBERSTON, J., SCHAAAKE, J. (Eds.), American Geophysical Union. 107–135.
- CISISZAR, I., GUTMAN, G. (1999), *Mapping global land surface albedo from NOAA AVHRR*. J.Geophys. Res. 104, 6215–6228.
- DE BRUIN, H.A.R., RONDA, R.J., VAN, DE., WEIL, B.J.H. (2000), *Approximate solution for the Obukhov length and surface fluxes in terms of bulk Richardson numbers*. Bound.-Layer. Meteorol. 95, 145–157.
- DICKINSON, R.E., HENDERSON SELLERS, A. (1988), *Modelling tropical deforestation: a study of GCM land-surface parameterizations*. Quart. J. R. Meteorol. Soc. 114, pp. 439–462.
- DUDHIA, J. (1989), *Numerical study of convection observed during the winter monsoon experiment using a mesoscale two-dimensional model*, J. Atmos. Sci. 46, 3077–3107.
- DUDHIA, J. (1996), A multi-layer soil temperature model for MM5. Preprints, The Sixth PSU/NCAR Mesoscale Model Users' Workshop, 22–24 July 1996, Boulder, Colorado, 49–50.
- DYER, A.J. (1974), *A review of flux-profile relationships*. Bound.-Layer. Meteorol. 20, 35–49.
- DYER, A.J., HICKS, B.B. (1970), *Flux-gradient relationships in the constant flux layer*. Quart. J. R. Meteorol. Soc. 96, 715–721.
- FRANK, D.C., ESPER, J., RAIBLE, C.C., BUNTGEN, U., TROUET, V., STOCKER, B., JOOS, F. (2010), *Ensemble reconstruction constraints on the global carbon cycle sensitivity to climate*. Nature. 463, 527–530.
- GOEL, M., SRIVASTAVA, H.N., 1990. *Monsoon Trough Boundary Layer Experiment (MONTBLEX)*. Bull. Amer. Meteor. Soc. 71, 1594–1600.
- GOSWAMI, P., RAMESH, K. V. (2008), *The expanding Indian desert: assessment through weighted epochal trend ensemble*. Curr. Sci., 94, 476–480.
- GUTMAN, G., IGNATOV, A. (1997), *The derivation of green vegetation fraction from NOAA/AVHRR data for use in numerical weather prediction models*. Int. J. Remote Sens. 19, 1533–1543.
- HONG, S.Y., NOH, Y., DUDHIA, J. (2006), *A new vertical diffusion package with an explicit treatment of entrainment processes*. Mon. Weather. Rev. 134, 2318–2341.
- HUIZHI, L., and JIANWU, F. (2012), *Seasonal and interannual variations of evapotranspiration and energy exchange over different land surfaces in a semiarid area of China*. J. Appl. Meteor. Climatol., 51, 1875–1888.
- JIMENEZ, P.A., DUDHIA, J., GONZALEZ-ROUCO, F., NAVARRO, J., MONTAVEZ, J.P., GARCIA-BUSTAMANTE, E. (2012), *A revised scheme for the WRF surface layer formulation*. Mon. Weather Rev. 140, 898–918.
- KABAT, P., CLAUSSEN, M., DIRMEYER, P.A., GASH, J.H.C., de GUENNI, L.B., MEYBECK, M., PIELKE, R.A Sr., VÖRÖSMARTY, C.J., HUTJES, R.W.A., LÜTKEMEIER, S. (2004), *Vegetation, water, humans and the climate: a new perspective on an interactive system*. Global change: the IGBP Series, Vol. 24, Springer Verlag, 566 pp.
- KAIN, J.S., FRITSCH, J.M. (1993), *Convective parameterization for mesoscale models: the Kain-Fritsch scheme*. In: EMANUEL, K.A., RAYMOND, D.J. (Eds.), The representation of cumulus convection in numerical models. American Meteorological Society, Boston.
- KAR, S.C., MALI, P., ROURAY, A. (2014), *Impact of land surface processes on the South Asian monsoon simulations using WRF modeling system*. Pure. Appl. Geophys. 171(9), 2461–2484. doi: 10.1007/s00024-014-0834-7.
- LEUNING, R., GORSELA, E.V., MASSMANB, W.J., ISAACC, P.R. (2012). *Reflections on the surface energy imbalance problem*. Agric For Meteorol. 156, 65–74.
- LIVNEH, B., RESTREPO, P.J., LETTENMAIER, D.P. 2011. *Development of a UniPed land model for prediction of surface hydrology and LandAtmosphere interactions*. J. Hydrometeorol. 00, 1–22.
- MIAO, J.F., WYSER, K., CHEN, D., RITCHIE, H. (2009), *Impacts of boundary layer turbulence and land surface process parameterizations on simulated sea breeze characteristics*. Ann. Geophys. 27, 2303–2320.
- MLAWER, E.J., TAUBMAN, S.J., BROWN, P.D., IACONO, M.J., CLOUGH, S.A. (1997), *Radiative transfer for inhomogeneous atmosphere: RRTM, a validated correlated-k model for the longwave*. J. Geophys. Res. 102, 16663–16682.
- MORAN, M.S., CLARKE, T.R., KUSTAS, W.P., WELTZ, M., AMER, S.A. (1994), *Evaluation of hydrologic parameters in a semi-arid rangeland using remotely sensed spectral data*. Water Resour. Res. 30(5), 1287–1297.
- NIYOGI, D., KISHTAWAL, C., TRIPATHI, S., GOVINDARAJU, R.S. (2010), *Observational evidence that agricultural intensification and land use change may be reducing the Indian summer monsoon rainfall*. Water Resour. Res., 46, W03533, doi:10.1029/2008WR007082.
- NOH, Y., CHEON, W. G., HONG, S. Y., RAASCH, S. (2003), *Improvement of the K-profile model for the planetary boundary layer based on large eddy simulation data*. Bound.-Layer Meteorol. 107, 401–427.
- PAULSON, C.A. (1970), *The mathematical representation of wind speed and temperature profiles in the unstable atmospheric surface layer*. J. Appl. Meteorol. 9, 857–861.
- RAHMANI, A.R., SONI, R.G. (1997), *Avifaunal changes in the Indian Thar Desert*. J. Arid Environ. 36 (4), 687–703.
- RAJA, P., BHATTACHARYA, B K., SINGH, N., SINHA, N.K., SINGH, J.P., PANDEY, C.B., PARIHAR, J.S. and ROY, M.M. (2013), *Surface energy balance and its closure in arid grassland ecosystem: a case study over Thar Desert*. J. Agrometeorol. spl.issue.Vol.1, pp.94–99.

- RAVI, S., HUXMAN, T.E. (2009), *Land degradation in the Thar Desert*. Front. Ecol. Environ. 7, 517–518. <http://dx.doi.org/10.1890/09.WB.029>.
- SANJAY, J. (2008), *Assessment of atmospheric boundary-layer processes represented in the numerical model MM5 for a Clear Sky Day using LASPEX observations*. Bound.-Layer Meteorol. 129, 159–177.
- SHYAMPURA, R.L., SINGH, S.K., SINGH, R.S., JAIN, B.L., GAJBHIYE, K.S. (2002), Soil Series of Rajasthan, NBSS & LUP publication. 95, pp.364. National Bureau of Soil Survey & Land Use Planning, Nagpur.
- SIKKA, D.R., NARASIMHA R. (1995), *Genesis of the monsoon trough boundary layer experiment (MONTBLEX)*, Proceedings of Indian Academy of Science. 104, 157–187.
- SKAMAROCK, W.C., KLEMP, J.B., DUDHIA, J., GILL, D.O., BARKER, D.M., DUDA, M.G., HUANG, X.Y., WANG, W., POWERS, J.G. (2008), A description of the advanced research WRF Version 3. NCAR Technical Note, NCAR/TN-475 + STR. Mesoscale and Microscale Meteorology Division, National Center for Atmospheric Research, Boulder.
- SRINIVAS, C.V., RAO, D.V.B., HARIPRASAD, D., HARI PRASAD, K.B.R.R., BASKARAN, R., VENKATRAMAN, B. (2014), *A study on the influence of the land surface processes on the Southwest Monsoon simulations using a regional climate model*. Pure Appl. Geophys. doi: [10.1007/s00024-014-0905-9](https://doi.org/10.1007/s00024-014-0905-9).
- STEWART, J.B., KUSTAS, W.P., HUMES, K.S., NICHOLS, W.D., MORAN, M.S. DE BRUIN, H.A.R. (1994), *Sensible heat flux-radiometric surface temperature relationship for 8 semi-arid areas*. J. Appl. Meteorol. 33, 11 10–1 117.
- TEWARI, M., CHEN, F., WANG, W., DUDHIA, J., LEMONE, M. A., MITCHELL, K., EK, M., GAYNO, G., WEGIEL, J., CUENCA, R. H. (2004), *Implementation and verification of the unified NOAA land surface model in the WRF model*. 20th conference on weather analysis and forecasting/16th conference on numerical weather prediction, pp. 11–15.
- UNLAND, H.E., HOUSER, P.R., SHUTTLEWORTH, W.J., YANG, Z.L. (1996), *Surface flux measurement and modeling at a semi-arid Sonoran Desert site*. Agric. For. Meteorol. 82, 119–153.
- USDA. (1994), Major world crop areas and climatic profiles. USDA Agricultural Handbook 664, 293 pp. [Available online at http://www.usda.gov/oce/weather/pubs/Other/MWCACP/world_crop_country.htm].
- VERNEKAR, K.G., SINHA, S., SADANI, L.K., SIVARAMAKRISHNAN, S., PARASNIS, S.S., MOHAN, B., DHARMARAJ, S., PATIL, M.N., PILLAI, J.S., MURTHY, B.S., DEBAJE, S.B., SINGH, A.B. (2003), *An overview of the land surface processes experiment (Laspex) over a semi-arid region of India*. Bound.-Layer Meteorol. 106, 561–572.
- WANG, A., BARLAGE, M., ZENG, X., DRAPER, C.S. (2014), *Comparison of land skin temperature from a land model, remote sensing, and in situ measurement*, J. Geophys. Res. Atmos. 119, 3093–3106, doi:[10.1002/2013JD021026](https://doi.org/10.1002/2013JD021026).
- WEBB, E. K. (1970), *Profile relationships: the log-linear range, and extension to strong stability*. Quart. J. R. Meteorol. Soc. 96, 67–90.
- XU, Q., QIU, C. J. (1997), *A variational method for computing surface heat fluxes from ARM surface energy and radiation balance systems*. J. Appl. Meteorol. 36, 4–11.
- YANG, Z.-L. (2004) Modeling land surface processes in short term weather and climate studies, in Observation, Theory and Modeling of Atmospheric Variability, edited by X. ZHU, X. LI, M. CAI, S. ZHOU, Y. ZHU, F.-F. JIN, X. ZOU, and M. ZHANG, World Scientific Series on Meteorology of East Asia, World Scientific, New Jersey, pp. 288–313.
- ZENG, X., WANG, Z., WANG, A. (2012), *Surface skin temperature and the interplay between sensible and ground heatfluxes over arid regions*. J. Hydrometeorol. 13, 1359–1370.
- ZHANG, D.L., ANTHES, R.A. (1982), *A high-resolution model of the planetary boundary layer—sensitivity tests and comparisons with SESAME-79 data*. J. Appl. Meteorol. 21, 1594–1609.
- ZHANG, Q., HUANG, R.H., WANG, S., et al. (2005), *NWC-ALIEX and its research advances*, Adv. Earth Sci. (in Chinese), 20, 427–441.
- ZHOU, L.T., WU, R.G., HUANG, R.H. (2010), *Variability of surface sensible heat flux over Northwest China*. Atmos. Oceanic Sci. Lett. 3, 75–80.

(Received August 1, 2015, revised December 7, 2015, accepted January 12, 2016, Published online February 2, 2016)